Received: 1 April 2020 | Revised: 12 June 2020 | Accepted: 16 June 2020

DOI: 10.1111/joa.13275

ORIGINAL ARTICLE

ANATOMICAL SOCIETY Journal of Anatomy WILEY

Anatomical relationship between the morphology of the styloid process of the ulna and the attachment of the radioulnar ligaments

Saya Horiuchi[1,2] | Akimoto Nimura[3] | Masahiro Tsutsumi[1] | Shiro Suzuki[3] | Koji Fujita[3] | Taiki Nozaki[1,2] | Keiichi Akita[1]

[1]Department of Clinical Anatomy, Graduate School of Medical and Dental Sciences, Tokyo Medical and Dental University, Tokyo, Japan

[2]Department of Radiology, St. Luke's International Hospital, Tokyo, Japan

[3]Department of Functional Joint Anatomy, Graduate School of Medical and Dental Sciences, Tokyo Medical and Dental University, Tokyo, Japan

Correspondence
Akimoto Nimura, Department of Functional Joint Anatomy, Graduate School of Medical and Dental Sciences, Tokyo Medical and Dental University, 1-5-45 Yushima, Bunkyo-ku, Tokyo 113-8519, Japan.
Email: nimura.orj@tmd.ac.jp

Funding information
JA Kyosai Research Institute; JSPS KAKENHI, Grant/Award Number: JP 19K18489

Abstract

The radioulnar ligaments are the major stabilizers of the distal radioulnar joint under dynamic loading; however, anatomical detail regarding their attachment on the middle and distal thirds of the styloid process of the ulna remains unclear. Because previous anatomical studies included only old cadavers, their anatomical findings might not reflect the morphological features of younger and healthy specimens. This study investigated the anatomical features of the distal ulna, particularly the styloid process, to determine the attachment of the radioulnar ligaments to the styloid process and verified their direction and attachment to the styloid process in younger and healthy donors using magnetic resonance imaging (MRI). We investigated the morphological features of the distal ulna of 12 cadaveric wrists using micro-computed tomography (micro-CT). We also visualized and measured the distribution of the cortical bone thickness. We histologically analyzed three specimens in the axial plane and macroscopically analyzed seven specimens to examine the attachment of the radioulnar ligaments to the styloid process. In addition, we evaluated five wrists from living volunteers using 3.0 Tesla MRI. The distal ulna has a ridge on the dorsoradial aspect of the styloid process that corresponds to the attachment of the radioulnar ligaments. Micro-CT images after data processing revealed that the cortical thickness of the dorsoradial quadrant was thicker than that of the other quadrant at the proximal slice of the styloid process ($p < 0.01$), and that of the dorsoulnar ($p = 0.021$) and ulnopalmar ($p < 0.01$) quadrants at the middle slice. Histological analyses showed that the radioulnar ligaments were attached to the middle and distal thirds of the styloid process via chondral-apophyseal entheses. The direction of the fiber was dorsal in the middle third of the styloid process and changed to palmar in the distal third of the styloid process. The direction and attachment of the radioulnar ligaments on the styloid process were confirmed using MRI for younger and healthy participants. The radioulnar ligaments were attached to the dorsoradial ridge of the styloid process, which was confirmed by cortical bone thickening, histology at the attachment

sites, and in vivo MR imaging. The directions of the radioulnar ligaments sterically intersected, which would satisfy both slipping stability and rotational mobility. These anatomical findings may provide the basis for biomechanical consideration of distal radioulnar joint stabilization.

KEYWORDS

dorsal, ligament, palmar, radius, triangular fibrocartilage complex, ulna, wrist

1 | INTRODUCTION

The triangular fibrocartilage complex stabilizes the distal radioulnar joint (Palmer and Werner, 1981). In particular, the radioulnar ligaments, which connect the disk proper and distal ulna, have been considered the major stabilizers of the distal radioulnar joint under dynamic loading (Bain *et al*., 2015; Haugstvedt *et al*., 2006; Nakamura and Makita, 2000; Rein *et al*., 2015). The fovea is important for the attachment of the radioulnar ligaments on the distal ulna; it is referred to as either the deep radioulnar ligament (Hagert, 1994) or the triangular ligament (Nakamura and Makita, 2000; Nakamura *et al*., 2001; Nakamura and Yabe, 2000; Nakamura *et al*., 1996). However, anatomical detail regarding the attachment of the radioulnar ligaments to the middle and distal thirds of the styloid process remains unclear (Hagert, 1994; Nakamura and Yabe, 2000; Ishii *et al*., 1998). Moreover, because previous anatomical studies included either aged cadavers (af Ekenstam and Hagert, 1985; Nakamura and Makita, 2000; Nakamura *et al*., 1996; Nakamura *et al*., 2001; Semisch *et al*., 2016) or specimens in which the age is unknown (Ishii *et al*., 1998; Palmer and Werner, 1981), these anatomical findings might not reflect the morphological features of younger and healthy specimens.

Bone is highly adaptive when undergoing mechanical stress loads (Wolff, 1892). Previous reports have described that high tensile stresses via dense connective tissues, such as the tendon, ligament, and aponeurosis, affect the morphology and cortical bone thickness of the attachment (Tamaki *et al*., 2014; Nozaki *et al*., 2015; Norman *et al*., 2017; Sato *et al*., 2018). The distal ulna is known to be shaped by the cartilage surface, fovea, sulcus of the extensor carpi ulnaris, and styloid process. However, the morphological features of the distal ulna, particularly the styloid process, concerning the tensile stress of the radioulnar ligaments, have rarely been discussed. These morphological features could potentially identify the mechanically active part of the attachment of the radioulnar ligaments to the styloid process.

The first aim of this study was to characterize the anatomical features of the distal ulna using bony morphological, histological, and macroscopic methods. The second aim was to verify the direction and attachment of the radioulnar ligaments to the styloid process in younger and healthy donors using magnetic resonance imaging (MRI). We hypothesized that the distal ulna, particularly the styloid process, would have anatomical characteristics that correspond to the attachment of the radioulnar ligaments, and that the findings could be visualized in vivo using MRI.

2 | MATERIALS AND METHODS

2.1 | Specimen preparation and micro-computed tomography imaging

Thirteen wrists, including hands from nine Japanese cadavers, were obtained for this study. All cadavers were donated to the Department of Anatomy of the Tokyo Medical and Dental University. The study design was approved by the Ethics Committee at our institution.

We fixed all cadavers in 8% formalin and preserved them in 30% ethanol. Specimens with remarkable deformation around the distal radioulnar joint or remarkable instability of the distal radioulnar joint were excluded. We sectioned all specimens to obtain the wrist using a diamond band pathology saw (EXAKT 312; EXAKTAdvanced Technologies). We obtained three-dimensional images of the 13 wrist blocks using a micro-computed tomography (micro-CT) scanner (inspeXio SMX-100 CT; SHIMADZU) and application software (VGStudio Max 2.0). The micro-CT parameters were as follows: voltage 100 kV, current 80 μA current, source-to-detector distance 700 mm, source-to-rotation center distance 500 mm, pitch 0.179, slice thickness 0.200 mm, field of view (xy) 91.55 mm, field of view (z) 45.0 mm, matrix 512 x 512, voxel size 0.179 mm/voxel. After obtaining three-dimensional images, one specimen was found to have severe calcification on the distal ulna. Therefore, we used 12 specimens (three right and nine left) from nine cadavers (two males and seven females; average age, 83.6 years; age range, 49–96 years) for the analyses.

2.2 | Cortical thickness mapping of the styloid process of the ulna

To visualize the distribution of the cortical bone thickness on the styloid process of the ulna, we utilized 8-bit images of the 12 specimens obtained as described previously. Image J open source image processing software (National Institutes of Health) and the plugin BoneJ (Doube *et al*., 2010) were used to define the thickness at a point by measuring the diameter of the greatest sphere that fit within the structure of interest (Kleinman, 2007; Doube *et al*., 2010). The cortical bone thickness of the styloid process of the ulna was mapped in three dimensions. Thicker points of the cortical bone were represented by brighter colors. We observed the dorsal, radial, palmar, and ulnar aspects of the styloid process.

To quantify the cortical bone thickness of the styloid process, we used axial images that were colored to indicate thickness. Each styloid

process was divided into four quadrants using two lines drawn through the center of the styloid process: one line drawn parallel to the palmar-to-dorsal long axis of the ulnar head, and another line drawn perpendicular to the dorsoradial, dorsoulnar, palmoradial, and palmoulnar quadrants. Two radiologists (SH and TN) independently measured the maximal cortical bone thickness in each quadrant at the proximal third, middle third, and distal third slices of the styloid process. An observer (SH) repeated the measurements in a random order to determine intra-observer reproducibility. We calculated the means and standard deviations of the maximal cortical bone thicknesses of the quadrants.

2.3 | Histological analysis

We used three wrist blocks for the histological analysis. We decalcified the samples for 1 week in a solution containing aluminum chloride, hydrochloric acid, and formic acid, as described previously (Plank and Rychlo, 1952). After decalcification, we dehydrated the blocks with a graded ethanol series, embedded them in paraffin, and serially sectioned them every 300 μm (thickness of 5 μm) parallel to the axial plane. We stained sections with Masson trichrome according to the methodology of a previous study of radioulnar ligament attachments (Benjamin *et al*., 1990).

2.4 | Macroscopic observations

We used seven wrist blocks for macroscopic observations. We removed the lunate and triquetrum bones from the blocks to preserve the pisiform bone and dorsal and palmar joint capsules. We separated the dorsal and palmar joint capsules from the peripheral margin of the disk proper to observe the attachment of the radioulnar ligaments to the styloid process of the ulna.

2.5 | In vivo imaging of younger aged participants based on MRI

To verify the histological findings of the cadaveric analyses, we evaluated right asymptomatic wrists from five living volunteers (three males and two females; average age, 34.2 years; age range, 30–42 years) using 3.0 Tesla MRI scanner (Discovery 750, GE Healthcare) and an eight-channel wrist coil. The study design was approved by the Ethics Committee at our institution. The proton density-weighted images were acquired in the axial plane using repetition time/echo time (TR/TE) 1800/36 ms, 400 × 400 matrix, 7-cm field of view (FOV), 1.0-mm sections, echo train length (ETL) 6, and receiver bandwidth 62.5 kHz.

2.6 | Statistical analyses

All statistical analyses were performed using R version 3.3.2 for Mac (R Development Core Team). The Kruskal–Wallis one-way analysis of variance test was used to compare the maximal cortical bone thicknesses of the quadrants between the proximal, middle, and distal slices. When significant differences among quadrants were evident, between-group comparisons were performed using the Steel–Dwass post hoc test. Significance was set at $p < 0.05$. Intra- and inter- observer reliability was assessed using intraclass correlation coefficients (ICCs).

3 | RESULTS

3.1 | Analysis of the bony configuration of the distal ulna using micro-CT

Using micro-CT, we identified the ridge on the dorsoradial aspect of the styloid process and depression on the palmar part of the ulnar fovea in all specimens (Figure 1). Using cortical thickness mapping of the micro-CT data, we found that the brightly colored area of the middle of the styloid process, which indicated a thicker cortical area, corresponded to the dorsoradial ridge of the styloid process (Figure 2a-c). At the proximal slice of the ulnar styloid process, the cortical thickness of the dorsoradial quadrant was thicker than that of the other quadrants (Figure 2d, $p < 0.01$ in Table 1). At the middle slice, the thickness of the dorsoradial quadrant was thicker than that of the dorsoulnar ($p = 0.021$) and ulnopalmar ($p < 0.01$) quadrants (Figure 2e). At the distal slice, there was no differences in quadrants (Figure 2f). All data are shown in Table 1. The inter- and intra-observer agreements for the measurements were excellent

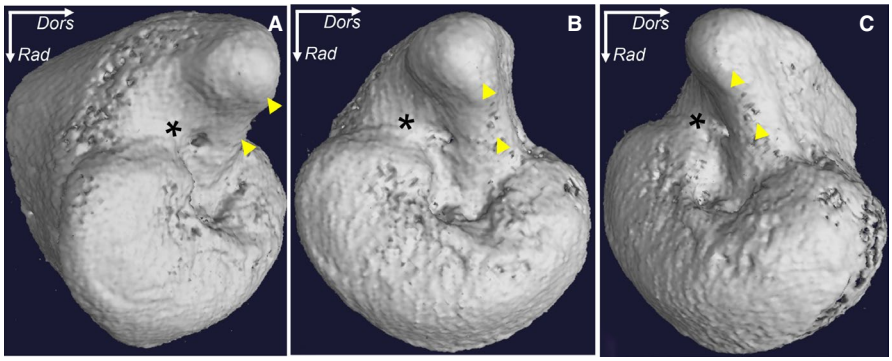

FIGURE 1 Bony morphology of the distal ulna with three-dimensional images obtained using micro-CT. Palmar-radial (a), radial (b), and dorsoradial (c) views of the distal end of the right ulna. The ridge on the dorsoradial aspect of the styloid process (yellow arrow heads) and depression on the palmar side of the distal ulna (asterisks) can be identified. *Dors*, dorsal; *Rad*, radial

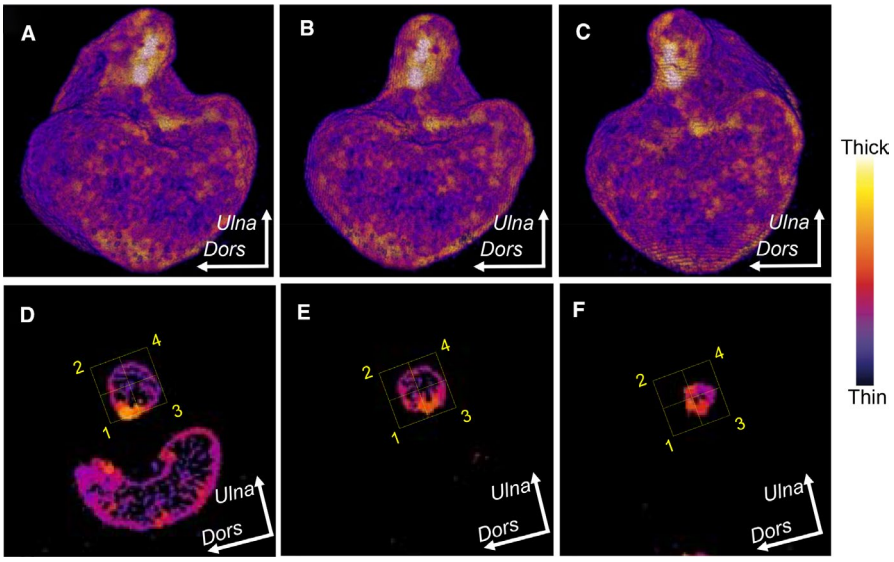

FIGURE 2 Evaluation of cortical bone thickening on the styloid process of the ulna. Cortical thickening maps of the styloid process of the left ulna visualized after image processing. Three-dimensional reconstructions show (a) dorsoradial, (b) radial, and (c) radiopalmar aspects of the styloid process. The thicker the cortical bone of the point, the brighter the color of the point. (d, e, f) Axial two-dimensional images of the styloid process are colored according to the thickness. The proximal third (d), middle third (e), and distal third (f) slices are shown. Each styloid process was quartered into dorsoradial (1), dorsoulnar (2), radiopalmar (3), and ulnopalmar (4) quadrants. The color bar indicates the thickness. *Dors*, dorsal; *Ulna*, ulnar

TABLE 1 Maximal cortical thickness

	Quadrant			
	Dorsoradial (1)	Dorsoulnar (2)	Radiopalmar (3)	Ulnopalmar (4)
Measurement level	Average and standard deviation (mm)			
Proximal third	1.05 ± 0.25*	0.65 ± 0.14	0.74 ± 0.14	0.60 ± 0.14
Middle third	0.85 ± 0.11**	0.68 ± 0.12	0.73 ± 0.14	0.63 ± 0.10
Distal third	0.79 ± 0.17	0.75 ± 0.13	0.74 ± 0.14	0.67 ± 0.11

Note: Location of measurements is demonstrated in Figure 2.

*Statistically significant difference compared to other quadrants ($p < .01$ by Kruskal–Wallis one-way analysis of variance test with post hoc Steel–Dwass test).

**Statistically significant difference compared to the dorsoulnar ($p = .021$) and ulnopalmar ($p < .01$) quadrants.

(inter-observer: ICC, 0.84; 95% CI, 0.78–0.88; intra-observer: ICC, 0.92; 95% CI, 0.89-0.94).

3.2 | Histological observation of the radioulnar ligaments

To understand the histological significance of the ridge on the dorsoradial aspect of the styloid process, we examined the serially sectioned axial preparations in relation to the radioulnar ligaments (Figure 3). The fibers of the radioulnar ligaments were attached to the ulna via chondral-apophyseal entheses, which were densely stained (Figure 3c-i). At the middle third of the styloid process, the radioulnar ligaments arose from the palmar part of the disk proper and attached to the styloid process in a dorsal direction (Figure 3e,f). When more distally observed, the direction of the radioulnar ligaments gradually changed from a dorsal to a palmar direction. At the distal third of the styloid process, the radioulnar ligaments arose from the dorsal portion of the disk proper and attached to the styloid process in a palmar direction (Figure 3g-i).

3.3 | Macroscopic dissection of the ulnar attachment of the radioulnar ligaments

On the dorsal side, we were able to clearly separate the dorsal margin of the disk proper and dorsal joint capsule, including the floor of the extensor tendon sheath (Figure 4a,b). The radioulnar ligaments were attached to the styloid process, and the most superficial fibers were directed to the palmar joint capsule (Figure 4c). On the palmar

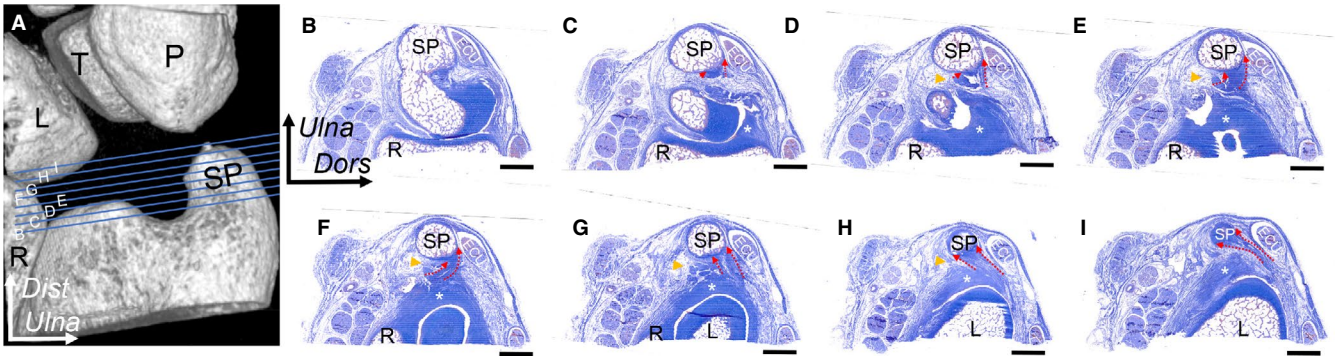

FIGURE 3 Histological analysis of the radioulnar ligaments using Masson's trichrome staining. Locations of the section are indicated as blue lines (a). (b-i) The radioulnar ligaments from the disk proper (asterisk) to the styloid process (SP) are indicated as red dotted arrows. The loose connective tissue is indicated as orange arrowheads. ECU, extensor carpi ulnaris tendon; L, lunate bone; P, pisiform bone; R, radius; T, triquetrum bone. *Dist*, distal; *Dors*, dorsal; *Ulna*, ulnar. Scale bars, 5 mm

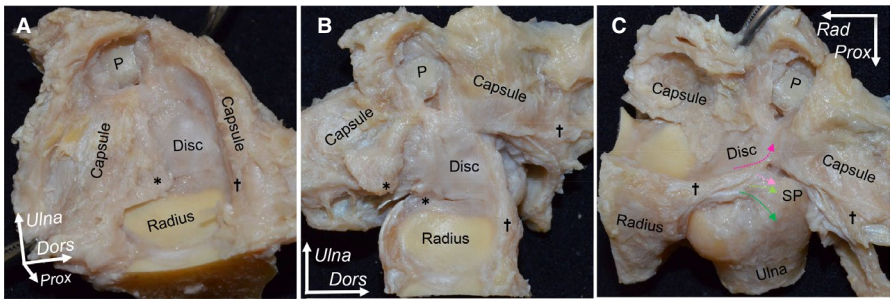

FIGURE 4 Macroscopic observation of the radioulnar ligaments. (a) The distal surface of the radius and the disk proper of the right wrist after removing the lunate and triquetrum. (b) The dorsal and palmar joint capsules were detached from the radius and peripheral margin of the disk proper. Daggers and asterisks indicate the same points before detachment. (c) The dorsal view of (b). Note the radioulnar ligaments (deep green, light green, and light pink dotted arrows) attached to the styloid process (SP) and the most superficial fibers directed to the palmar joint capsule (pink dotted arrow). *Dors*, dorsal; *Rad*, radial; *Prox*, proximal; *Ulna*, ulnar

side, the palmar and synovial joint capsules and disk proper were intermingled and could not be clearly separated. The most superficial fibers were connected from the disk proper and led to the palmar joint capsule, which was attached to the palmar side of the lunate and triquetrum and included the pisotriquetral joint.

3.4 | In vivo imaging of younger participants based on MRI

To verify the histological data, we observed the direction and attachment of the radioulnar ligaments to the styloid process (Figure 5). The radioulnar ligaments were visualized as cord-like structures of low intensity (Figure 5c-g). At the proximal half of the styloid process, the radioulnar ligaments arose from the palmar part of the disk proper and attached to the dorsoradial aspect of the styloid process in a dorsal direction (Figure 5c,d). In the more distal slices, the radioulnar ligaments arose from the dorsal portion of the disk proper and attached to the styloid process in a palmar direction (Figure 5e-g). The layers and directions of the radioulnar ligaments are summarized as schemes in Figure 6.

4 | DISCUSSION

The present study used micro-CT imaging of cadaveric specimens to reveal that the ridge on the dorsoradial aspect of the styloid process corresponded with cortical bone thickening. In addition, histological and macroscopic observations showed that the radioulnar ligaments were attached to the dorsoradial ridge of the styloid process via chondral-apophyseal entheses, and gradually changed from the dorsal to the palmar direction when observed more distally. Furthermore, MRI confirmed these structures in younger, living participants. Therefore, these findings supported our hypothesis that the styloid process has anatomical characteristics corresponding to the attachment of the radioulnar ligaments, which could be visualized in vivo using MRI.

The morphology of the distal end of the ulna has been described as having a head, styloid process, and depression that separate them referred to as the fovea (Quain and Thane, 1896; Standring, 2016). There have been no previous descriptions regarding the differences distinguishing the dorsal and palmar parts of the distal ulna, except for the bony groove of the extensor carpi ulnaris. In the present study, the three-dimensional images

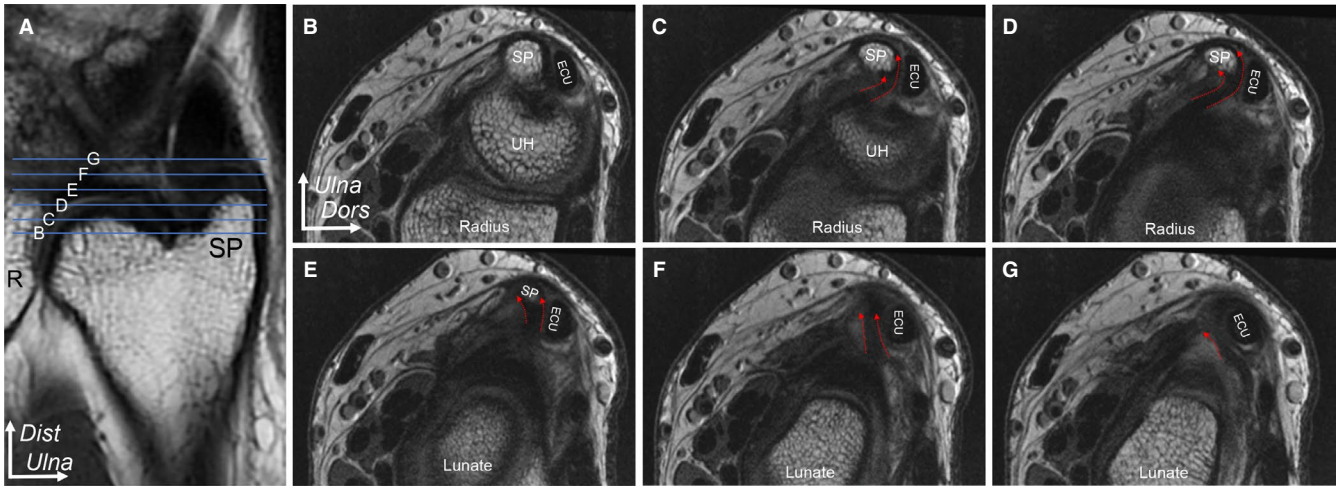

FIGURE 5 In vivo MR imaging of the attachment of the radioulnar ligaments on the styloid process in younger and healthy participants. Locations of the slices are indicated as blue lines (a). Axial slices of ulnar part of the wrist are shown (b-g). The radioulnar ligaments are indicated as red dotted arrows. ECU, extensor carpi ulnaris tendon; *Dist*, distal; *Dors*, dorsal; *Rad*, radial

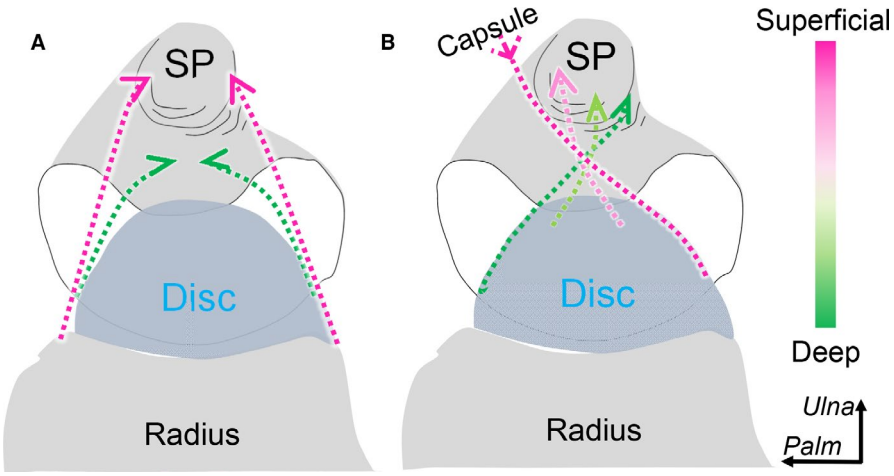

FIGURE 6 Comparison of the schematic illustrations of the direction and attachment of the radioulnar ligaments. These illustrations show the distal surface of the ulnar part of the radius, disk proper, and ulna. (a) Previous understanding of the symmetrical distribution of the radioulnar ligaments. (b) The current understanding of the asymmetrical distribution of the radioulnar ligaments based on the present study. The color bar indicates the depth of the radioulnar ligaments from green (deep) to pink (superficial). *Palm*, palmar; *Ulna*, ulnar

obtained using micro-CT revealed a ridge on the dorsoradial aspect of the styloid process and a depression on the palmar part of the fovea. These findings were validated by the fact that cortical bone thickening was limited in the dorsoradial part of the middle of the styloid process. As previously described, these bony morphological features, particularly cortical bone thickening, could correspond to the high tensile stress from the dense connective tissues (Tamaki *et al*., 2014; Nozaki *et al*., 2015; Norman *et al*., 2017; Sato *et al*., 2018).

Regarding the attachment of the radioulnar ligaments, anatomical knowledge of the following two areas has been separately discussed: (a) the fovea and base of the styloid process and (b) the middle and tip of the styloid process. The attachment of the radioulnar ligaments to the fovea has been verified and is referred to as the deep part of the radioulnar ligaments or the triangular ligament (Nakamura and Makita, 2000; Nakamura *et al*., 2001; Nakamura and Yabe, 2000; Nakamura *et al*., 1996). However, the attachment to the middle and tip of the styloid process has been controversial. The superficial parts of the radioulnar ligaments are reportedly attached to the distal part of the styloid process (Hagert, 1994; Ishii *et al*., 1998). Conversely, it has been reported that there is loose connective tissue interposed between the disk proper and the middle of the styloid process (Nakamura and Yabe, 2000). Here, we found that the radioulnar ligaments are attached to the styloid process via chondral-apophyseal entheses, with gradual changes from the dorsal in the middle third of the styloid process, to the palmar direction in the distal third. These results are supported by Semisch *et al*. (2016), who reported that

fibrocartilage was found at the ulnar styloid insertion between the radioulnar ligaments and bone.

Controversy regarding the attachment of the radioulnar ligaments on the styloid process could have two explanations: first, previous histological analyses were mainly focused on frontal sections, and rarely included axial sections. Based on the histological results of the present study, the fibers of the radioulnar ligaments attaching to the middle and tip of the styloid process comprised lamellar structures. Therefore, serial axial sections, particularly thin slices, could be more effective than frontal sections for observing the gradual changes of the fibers.

Second, previous studies may have insisted on the anatomical concept of the radioulnar ligaments being clearly separated into deep and superficial parts based on the ligamentum subcruentum, as previously stated by Henle (1856). The ligamentum subcruentum could be interpreted as the loose connective tissue radial to the middle of the styloid process and interposed between the layers of the radioulnar ligaments attached to the styloid process (orange arrowheads in Figure 3). Macroscopic findings showed that the radioulnar ligaments could not be separated into the superficial and deep parts and were continuous structures attached to the styloid process. Previous studies have reported (Nakamura and Makita, 2000; Nakamura and Yabe, 2000) that the deep and superficial portions of the triangular fibrocartilage complex cannot be clearly divided, which supports our findings.

Our results have provided a clinically relevant new anatomical basis for biomechanical considerations of the distal radioulnar joint stabilizing. Previous studies have reported conflicting results regarding the direction in which tightening occurs. Ekenstam & Hagert (1985) reported that the palmar radioulnar ligament was taut in pronation, whereas Shuind et al. (1991) argued that the dorsal radioulnar ligament tightened in pronation. Later, Hagert (1994) explained that the superficial and deep layers of the radioulnar ligaments tightened in different directions. Importantly, though the directions of the radioulnar ligaments were previously assumed to be symmetrical and non-intersecting structures, we found they were asymmetrical and sterically intersected. These structures could be interpreted as analogous to the anterior and posterior cruciate ligaments of the knee, which have been phylogenetically preserved since reptiles (Bolk *et al*., 1938). It is thought that intersecting structures are better than non-intersecting structures in terms of satisfying both slipping stability and rotational mobility, where the joint would be stabilized better, but with worse rotation (Castaing and Burdin, 1979). These intersecting structures seem reasonable for the concept of "tensegrity," which requires stability through a synergy of ligament tensile and joint compressive force (Hagert & Hagert 2010), based on the highly innervated character of the radioulnar ligament (Rein *et al*., 2015). We hope the principal intrinsic stabilizers of the distal radioulnar joint will be reconsidered on the basis of our anatomical findings.

The present study had several limitations. First, only a few specimens were analyzed. Second, histological analyses were limited to axial sections. Therefore, the vertical attachment of the radioulnar ligaments to the fovea was not sufficiently observed to conclude. Nevertheless, other studies have shown the significance of the vertical attachment to the fovea (Nakamura and Makita, 2000; Hagert, 1994; Nakamura *et al*., 2001; Nakamura and Yabe, 2000; Nakamura *et al*., 1996; Ishii *et al*., 1998; Berger, 1997; Garcia-Elias and Domenech-Mateu, 1987), and we have contributed new findings regarding the attachment of the radioulnar ligaments to the ulnar styloid in the axial dimension.

In conclusion, we observed that the styloid process of the distal ulna had a ridge on its dorsoradial aspect, corresponding to the chondral-apophyseal entheses of the radioulnar ligaments. The directions of the radioulnar ligaments were sterically intersected, which may better satisfy both slipping stability and rotational mobility.

ACKNOWLEDGEMENTS

This study was supported by JSPS KAKENHI (grant number JP 19K18489) and JA Kyosai Research Institute (Agricultural Cooperative Insurance Research Institute).

CONFLICT OF INTERESTS

None.

AUTHOR CONTRIBUTIONS

S.H.: Study design, acquisition of data, data analysis and interpretation, and drafting of the manuscript. A.N.: Supervising the work, critical revision of the manuscript. M.T.: Data analysis and interpretation. S.S.: Concept and design. K.F.: Critical revision of the manuscript. T.N.: Acquisition of data, and critical revision of the manuscript. K.A.: Supervising the work and commenting on drafts and the final version of the manuscript.

DATA AVAILABILITY STATEMENT

Research data are not shared.

ORCID

Akimoto Nimura https://orcid.org/0000-0002-3054-0273
Masahiro Tsutsumi https://orcid.org/0000-0003-1803-8202

REFERENCES

Bain, G.I., Eng, K., Lee, Y.C., Mcguire, D. and Zumstein, M. (2015) Reconstruction of chronic foveal TFCC tears with an autologous tendon graft. *Journal of Wrist Surgery*, 4(1), 9–14.

Benjamin, M., Evans, E.J. and Pemberton, D.J. (1990) Histological studies on the triangular fibrocartilage complex of the wrist. *Journal of Anatomy*, 172, 59–67.

Berger, R.A. (1997) The ligaments of the wrist. A current overview of anatomy with considerations of their potential functions. *Hand Clinics*, 13(1), 63–82.

Bolk, L., Göppert, E., Kallius, E. and Lubosch, W. (1938) *Handbuch der vergleichenden anatomie de wirbeltiere*. Berlin, Wien: Urban & Schwarzenberg.

Castaing, J. and Burdin, P. (1979) Le Genou. *Anatomie fonctionnelle de l'appareil locomoteur*. Paris, France: Vigot.

Doube, M., Klosowski, M.M., Arganda-Carreras, I., Cordelières, F.P., Dougherty, R.P., Jackson, J.S., Schmid, B., Hutchinson, J.R. and Shefelbine, S.J. (2010) BoneJ: Free and extensible bone image analysis in ImageJ. *Bone*, 47(6), 1076–1079.

Ekenstam, F.A. and Hagert, C.G. (1985) Anatomical studies on the geometry and stability of the distal radio ulnar joint. *Scandinavian Journal of Plastic and Reconstructive Surgery*, 19(1), 17–25.

Garcia-Elias, M. and Domenech-Mateu, J.M. (1987) The articular disc of the wrist. Limits and relations. *Acta Anatomica*, 128(1), 51–54.

Hagert, C.G. (1994) Distal radius fracture and the distal radioulnar joint–anatomical considerations. *Handchirurgie, Mikrochirurgie, Plastische Chirurgie*, 26(1), 22–26.

Hagert, E. and Hagert, C.G. (2010) Understanding stability of the distal radioulnar joint through an understanding of its anatomy. *Hand Clinics*, 26(4), 459–466.

Haugstvedt, J.R., Berger, R.A., Nakamura, T., Neale, P., Berglund, L. and An, K.-N. (2006) Relative contributions of the ulnar attachments of the triangular fibrocartilage complex to the dynamic stability of the distal radioulnar joint. *Journal of Hand Surgery*, 31(3), 445–451.

Henle, J. (1856) *Handbuch der Bänderlehre des Menschen*. Braunschweig, Germany: Friedrich Vieweg.

Ishii, S., Palmer, A.K., Werner, F.W., Short, W.H. and Fortino, M.D. (1998) An anatomic study of the ligamentous structure of the triangular fibrocartilage complex. *Journal of Hand Surgery*, 23(6), 977–985.

Kleinman, W.B. (2007) Stability of the distal radioulna joint: biomechanics, pathophysiology, physical diagnosis, and restoration of function what we have learned in 25 years. *Journal of Hand Surgery*, 32(7), 1086–1106.

Nakamura, T. and Makita, A. (2000) The proximal ligamentous component of the triangular fibrocartilage complex. *Journal of Hand Surgery*, 25(5), 479–486.

Nakamura, T., Takayama, S., Horiuchi, Y. and Yabe, Y. (2001) Origins and insertions of the triangular fibrocartilage complex: a histological study. *Journal of Hand Surgery*, 26(5), 446–454.

Nakamura, T. and Yabe, Y. (2000) Histological anatomy of the triangular fibrocartilage complex of the human wrist. *Annals of Anatomy-Anatomischer Anzeiger*, 182(6), 567–572.

Nakamura, T., Yabe, Y. and Horiuchi, Y. (1996) Functional anatomy of the triangular fibrocartilage complex. *Journal of Hand Surgery*, 21(5), 581–586.

Norman, D., Metcalfe, A.J., Barlow, T., Hutchinson, C.E., Thompson, P.J.M., Spalding, T.J.W. and Williams, M.A. (2017) Cortical bony thickening of the lateral intercondylar wall: The functional attachment of the anterior cruciate ligament. *The American Journal of Sports Medicine*, 45(2), 394–402.

Nozaki, T., Nimura, A., Fujishiro, H., Mochizuki, T., Yamaguchi, K., Kato, R., Sugaya, H. and Akita, K. (2015) The anatomic relationship between the morphology of the greater tubercle of the humerus and the insertion of the infraspinatus tendon. *Journal of Shoulder and Elbow Surgery*, 24(4), 555–560.

Palmer, A.K. and Werner, F.W. (1981) The triangular fibrocartilage complex of the wrist—anatomy and function. *Journal of Hand Surgery*, 6(2), 153–162.

Plank, J. and Rychlo, A. (1952) A method for quick decalcification. *Zentralblatt für Allgemeine Pathologie und Pathologische Anatomie*, 89, 252–254.

Quain, J. and Thane, G.D. (1896) *Quaine's elements of anatomy*. London, UK: Longmans, Green, and Co.

Rein, S., Semisch, M., Garcia-Elias, M., Lluch, A., Zwipp, H. and Hagert, E. (2015) Immunohistochemical mapping of sensory nerve endings in the human triangular fibrocartilage complex. *Clinical Orthopaedics and Related Research*, 473(10), 3245–3253.

Sato, T., Nimura, A., Yamaguchi, R., Fujita, K., Okawa, A. and Akita, K. (2018) Intramuscular tendon of the adductor pollicis and underlying capsule of the metacarpophalangeal joint: An anatomical study with possible implications for the stener lesion. *Journal of Hand Surgery*, 43(7), 682 e681–682 e688.

Schuind, F., An, K.N., Berglund, L., Rey, R., Cooney, W.P., Linscheid, R.L. and Chao, E.Y.S. (1991) The distal radioulnar ligaments: a biomechanical study. *Journal of Hand Surgery*, 16(6), 1106–1114.

Semisch, M., Hagert, E., Garcia-Elias, M., Lluch, A. and Rein, S. (2016) Histological assessment of the triangular fibrocartilage complex. *Journal of Hand Surgery*, 41(5), 527–533.

Standring, S. (2016) *Gray's anatomy: the anatomical basis of clinical practice*. Philadelphia, PA: Elsevier Limited.

Tamaki, T., Nimura, A., Oinuma, K., Shiratsuchi, H., Iida, S. and Akita, K. (2014) An anatomic study of the impressions on the greater trochanter: bony geometry indicates the alignment of the short external rotator muscles. *Journal of Arthroplasty*, 29(12), 2473–2477.

Wolff, J. (1892) *Das Gesetz der Transformation der Knochen*. Berlin, Germany: August Hirschwald.

How to cite this article: Horiuchi S., Nimura A., Tsutsumi M., Suzuki S., Fujita K., Nozaki T., Akita K. Anatomical relationship between the morphology of the styloid process of the ulna and the attachment of the radioulnar ligaments. *J. Anat*. 2020;237:1032–1039. https://doi.org/10.1111/joa.13275